Comparison of J-integral from single specimen SE(T) tests on API-5L X100 line pipe steel

Conference Paper · June 2015

2 authors:

Timothy S. Weeks
National Institute of Standards and Technolo…
10 PUBLICATIONS **23** CITATIONS
SEE PROFILE

D. T. Read
National Institute of Standards and Technolo…
111 PUBLICATIONS **1,225** CITATIONS
SEE PROFILE

Comparison of *J*-integral from single specimen SE(T) tests on API-5L X100 line pipe steel

T.S. Weeks
National Institute of Standards and Technology
Boulder, CO, USA

D.T. Read
FFS Materials
Boulder, CO, USA

ABSTRACT

The clamped single-edge notched tension (SE(T)) specimen has seen increased use as a single-specimen testing scheme to determine tearing resistance curves in high strength steel pipe. The SE(T) specimen with appropriate notch geometry is a low-constraint specimen designed to reduce conservatism in the toughness measurement when compared to other toughness testing methods. The *J*-integral is robust and simple to calculate from data obtained by the use of several direct experimental measurements. This study employed a wide variety of instrumentation on API 5L X100 SE(T) specimens with fixed test parameters for direct comparison. This paper presents the details of the instrumentation and determination of the *J*-integral used in developing resistance curves. The results of this study show that directly measuring strain gradients can yield commensurate results to other non-codified methods currently under development for evaluating *J*-resistance curves in pipeline steels. Such experimental comparisons are needed to assure that the analysis methods used in both test-method development and in structural analysis accurately simulate the actual material behavior. Because the high fracture toughness of modern pipeline steels allows the development of extensive strain fields before significant tearing, practical strain gradient measurement techniques with local strain capacity up to 20 % will be needed to more accurately quantify the comparison between calculations and experiment. To the authors' knowledge this direct comparison has never been conducted and published by use of independent instrumentation on the same specimens.

KEY WORDS: SE(T), SENT, *J*-integral, pipelines, ductile tearing, fracture toughness

INTRODUCTION

Commonly used fracture mechanics test standards, such as ASTM E1820-13 (ASTM, 2013), BS 7448-1(BSI, 1991) and ISO 12135 (ISO, 2007), mainly address the measurement of fracture toughness by use of high constraint laboratory specimens, such as compact tension C(T), single edge-notched bend SE(B), and disk-shaped compact tension DC(T). ASTM E1820 has an appendix to support low-constraint shallow cracked SE(B) specimens. High-constraint (deep-cracked) specimens provide more conservative (*i.e.*, lower) toughness values than low-constraint (shallow-cracked) specimens; however, in general, bend specimens provide higher constraint than tension specimens at the same crack depth. The lower constraint at the crack tip in SE(T) specimens enhances crack growth resistance. The effects of increasing constraint for the same loading mode are observed when comparing clamped SE(T) specimens with shallow cracks ($a/W \approx 0.25$) and deep cracks ($a/W \approx 0.45$ (Tang et al., 2010), $a/W \approx 0.5$ (Park et al., 2011a, 2011b)). However, the parametric influence on toughness values for the purpose of a reasonable comparison between specimen geometry, flaw geometry and loading mode remains elusive *sans* standardized testing procedures. The definition of constraint and methods of parameterizing it has received substantial attention for the purpose of testing constraint designed small scale specimens where transferability is of paramount importance (Chao, Yang, & Sutton, 1994; Chao & Zhu, 2000; Joyce & Link, 1995, 1997; Kim, 2001; Liu & Chao, 2003; Mathias, Sarzosa, & Ruggieri, 2013a, 2013b; Ruggieri, 2012a, 2012b; Sarzosa & Ruggieri, 2013; Silva, Cravero, & Ruggieri, 2006; Zhu & Joyce, 2012). The majority of the work referenced deals primarily with resistance to ductile crack extension. The goal of these investigations is to ultimately test and compare different materials and assess their suitability in structural applications.

Despite the lack of a consensus SE(T) testing standard, considerable research has been done recently on the SE(T) fracture specimen (Cravero & Ruggieri, 2007; Hertelé, Verstraete, Denys, & O'Dowd, 2014; Kalyanam et al., 2010; Mathias et al., 2013b; Paredes & Ruggieri, 2011; Park, Tyson, Gianetto, Shen, & Eagleson, 2010; Pisarski, 2010; Pisarski & Wignal, 2002; Pussegoda et al., 2013; Ruggieri, 2012b; Sarzosa & Ruggieri, 2013; Shen & Tyson, 2009; Tang et al., 2010; Verstraete, Hertelé, Denys, Van Minnebruggen, & De Waele, 2014; Wang, Zhou, Shen, & Duan, 2012; Zhu & McGaughy, 2014). There are three recommended practices currently in use to evaluate ductile crack propagation: the multi-specimen test (DNV-RP-F108, 2006), and two single-specimen tests (CanmetMATERIALS, 2010; ExxonMobil, 2010). Some recent results have been published comparing the multi-specimen method to a single-specimen method (Pussegoda et al., 2013).

The initial goal of this research was to compare the two single-specimen methods. From tests employing the two single-specimen methods

simultaneously on a common specimen, the methods were compared and are the subject of previously published reports (Weeks & Lucon, 2014; Weeks, McColskey, Read, & Richards, 2013). Supplementary instrumentation was introduced for future analysis in those papers. This paper presents the details of evaluating the *J*-integral by way of directly measured surface strain gradients (J_{SG}) and comparing the results to the *J*-integral evaluated by way of the crack mouth opening displacement (CMOD), now referenced as J_{CMOD}.

As previously in (Weeks & Lucon, 2014), the two single-specimen methods will be referred to as the *J*-R method and the CTOD-R method. The *J*-R and CTOD-R methods were sourced from the recommended practices published by CanmetMATERIALS, Natural Resources Canada (CanmetMATERIALS, 2010) and ExxonMobil Upstream Research Company (ExxonMobil, 2010), respectively, and define the specimen geometry, notch geometry, crack geometry, general experimental setup, loading profile and analysis of the data.

Both methods effectively determined the same CMOD throughout the test regardless of the amount of ductile crack extension. Both referenced methods use CMOD elastic unloading compliance (UC) to determine the amount of crack extension. It is for this reason that the *J*-integral evaluated here, J_{SG}, will only be compared to the *J*-integral derived by the *J*-R method referenced above, again denoted J_{CMOD}.

The experimental design, instrumentation, setup, and test procedure details were published previously (Weeks & Lucon, 2014; Weeks et al., 2013). Supplementary instrumentation included front- (notched side) and back-face extensometers, strain gage arrays and direct current potential drop (DCPD). The *Experimental Setup* section will further detail the front- and back-face extensometers as well as the strain gage arrays. For completeness, the details of the specimen material and geometry are also given in the *Experimental Setup* section.

The *J-integral from CMOD* and *J-integral from Surface Strains* sections detail the analysis methods and equations used to evaluate the *J*-integrals for correlation to CMOD and ultimately crack extension. The *Results* section presents the *J*-integral from both methods for each specimen tested. The *Discussion* section describes the comparisons as well as complexities encountered in this research. Finally some observations regarding the critical parameters influencing the results conclude this paper.

EXPERIMENTAL SETUP

Material

Specimen blanks were cut in the axial direction from a section of 914 mm diameter, 19.1 mm wall thickness, API-5L X100 UOE pipe straddling the 3 o'clock position with respect to the seam weld. The tensile tests were performed at CanmetMATERIALS, with round bars cut from the four corners of the section of pipe used for the SE(T) tests. Measured values of yield strength and ultimate strength at room temperature were 745±8 MPa and 835±11 MPa, respectively, where all reported error bounds are plus or minus one standard deviation (Tyson & Gianetto, 2013).

Specimen Geometry

The testing performed here used square cross-section specimens ($B \times B$, $B=W$). The nominal thickness of each specimen was 17.5 mm. The initial crack size to thickness ratio (a_0/W) was set at 0.4 to match the crack size used by Tyson and Gianetto (2013) in the referenced *J*-R round-robin testing program.

The notches and integral knife-edges were machined with a continuous-wire electric-discharge machining (EDM) method. Three different notch-root radii were evaluated. One specimen had a 7 mm deep notch machined with a 0.1 mm diameter wire, resulting in a measured notch-root radius of 0.06 mm. Two specimens had 7 mm notches machined with a 0.25 mm diameter wire, resulting in a measured notch-root radius of 0.16 mm. The final two specimens were initially notched to 5 mm with the 0.25 mm diameter wire, but were then fatigue pre-cracked (notch-root radius assumed to be 0.0 mm) to 7 mm to obtain the prescribed a_0/W ratio of 0.4 for all specimens tested.

The notch geometries and integral knife-edge details are illustrated in Figure 1. Both sides of the specimens were side-grooved to 0.075*B* for a reduced total thickness of 0.85*B*. The details of the side grooves are shown in Figure 2. The net section thickness (*BN*) was 14.875 mm.
The length of each specimen was 315 mm (18*W*), which allowed for a grip-to-grip separation, *H*, of 175 mm (10*W*) and a grip length of 70 mm (4*W*) on each end of the specimen.

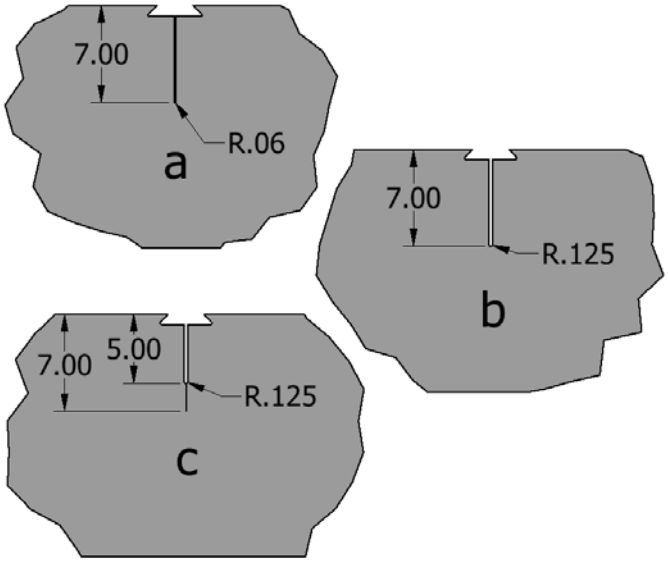

Figure 1. Notch geometry details for (a) 0.1 mm wire EDM, (b) 0.25 mm wire EDM and (c) fatigue pre-cracked specimens (all linear dimensions in mm). Note that dimensions given were provided for the purpose of machining and are not the as-tested condition, which require careful measurement prior to testing.

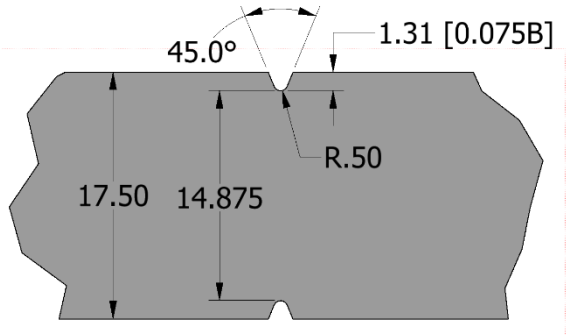

Figure 2. Details of the side grooves for each specimen. Total reduction in thickness is 0.15*B* (all linear dimensions in mm). Note that dimensions given were provided for the purpose of machining and are not the as-tested condition, which require careful measurement prior to testing.

Instrumentation

Strain gages were installed in two symmetric loops about the notch, as shown in Figure 3 and Figure 4. Two different strain gage configurations were used within each loop of 27 gages: single-element gages and miniature ten-element strip gages with independent grids. Each individual gage element in either configuration had an active gage length of 0.79 mm (0.031 in). The strain gage loops were installed to capture the strain gradients on the front-face and the back-face of each specimen along the axial centerline symmetrically about the notch-plane.

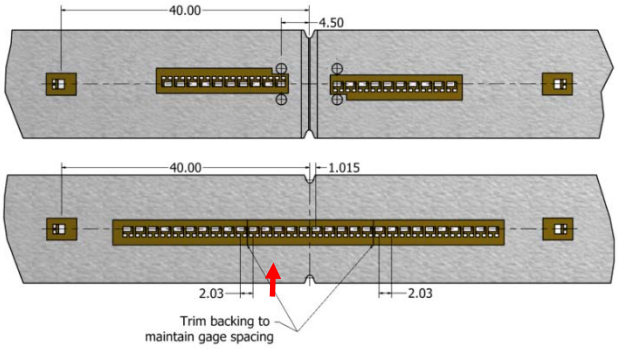

Figure 3. Details of strain gage placement on each specimen, (top) front-face gage placement and (bottom) back-face placement (all linear dimensions in mm). The red arrow points to SG #52 referenced later in the paper.

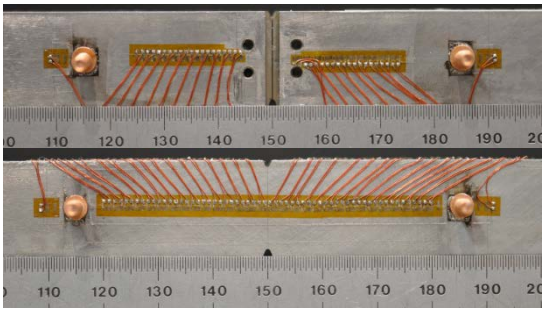

Figure 4. Photographs of (top) front-face strain gages installed and (bottom) back-face strain gages installed. Lead wire pairs for each gage are shown attached; each pair wraps around to the side of the specimen, where terminal strips are bonded to the surface of the specimen. Ribbon wires are soldered to the terminal strips.

A preliminary finite element analysis (FEA) was performed to determine the areas of the specimen with the largest surface strain gradients. Peak strains were predicted to be within ±20 mm of the crack path centerline (notch-plane) on the back-face of the specimen. The specimen was modeled as a bi-linear isotropic material with simple geometry, that is, without special notch-tip elements and with small strains. Results of this FEA are shown in Figure 5, which were used to determine the location of the strain gradient measurements with maximum resolution with respect to position.

To best capture this gradient, three ten-gage strips were installed on the back-face symmetrically about the notch-plane. The grid spacing of the ten-gage strips was 2.03 mm (0.08 in), defining the incremental resolution of the strain gradient measurement. The strain gage strips on the front-face were trimmed and placed so that the axial strain between the threaded holes could be measured. The gage strips were wired to terminal strips glued to the side of the specimen. Individual three-wire ribbons interconnected the conditioning and digital data acquisition system to the terminal strips to complete the individual circuits. Strain gage signals were zeroed at the start of each test.

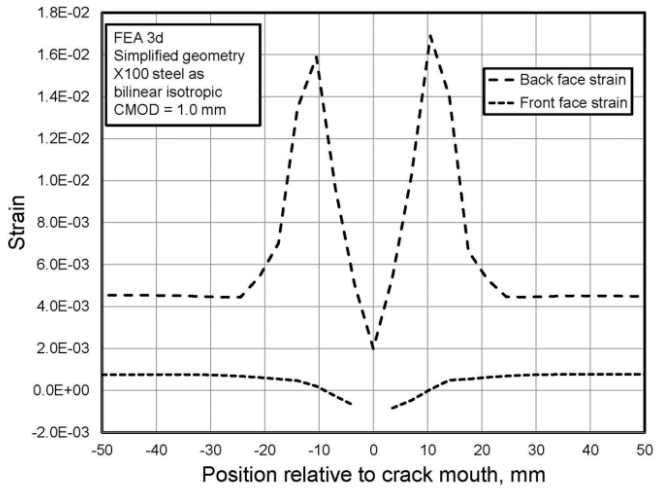

Figure 5. FEA output plot of Strain vs. Position for an X100 SE(T) specimen modeled as a bi-linear isotropic material at a CMOD of 1.0 mm. The maximum strain gradient shown here indicates that the best measurement resolution will be obtained with a focused measurement between ±20 mm symmetric about the notch-plane.

Threaded posts were installed on the front- and back-faces of the specimen for attachment of the extensometer mounting blocks. The posts were spaced 70 mm (4*W*) apart symmetric about the notch-plane and were attached by use of capacitive discharge welding to minimize disturbances in the strain field and load path away from the notch. An extensometer mounting block was installed on each post.
Figure 6 shows the layout and dimensions of the threaded posts as well as a view of the specimen with mounting blocks installed. The extensometers had a nominal gage length of 50 mm with a total calibrated travel of ± 6 mm. Extensometer signals were zeroed at the start of each test.

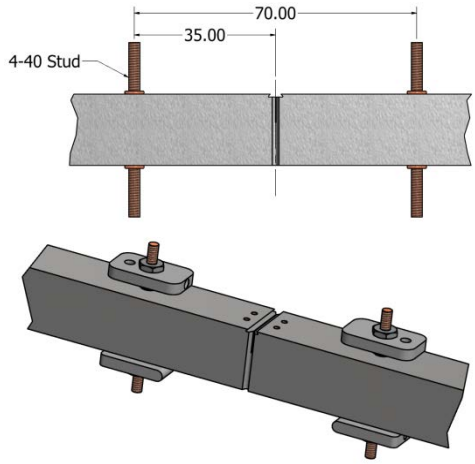

Figure 6. Details of the threaded post locations for the extensometer mounts; (top) side view with dimensions and (bottom) isometric view of the posts with blocks installed.

Primary instrumentation included the CMOD clip gage installed on the integral knife edges of the specimens. As previously reported and compared, the CMOD measurement was accompanied by two additional clip gages measuring the offset opening displacement by way of a double clip gage mounting fixture; not detailed in this paper. Other supplementary instrumentation also included DCPD also not detailed here. These details as well as others regarding the test procedure are given in (Weeks & Lucon, 2014). A photograph of a fully instrumented specimen is show in Figure 7.

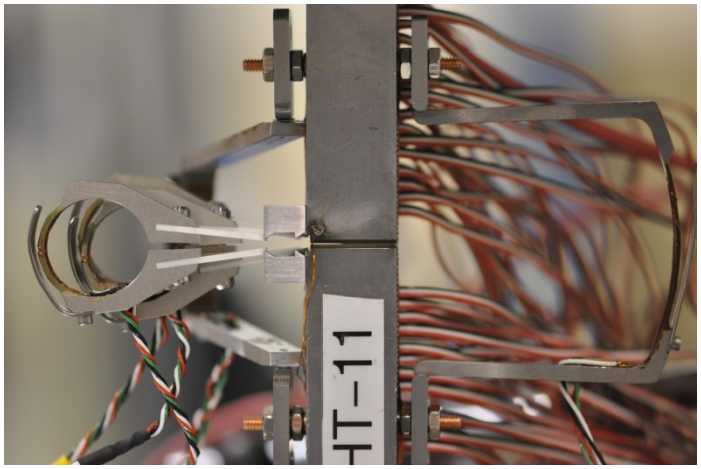

Figure 7. Side-view photograph of the HT-11 specimen fully instrumented immediately prior to testing.

J-INTEGRAL FROM CMOD

While the details of these equations and calculations have been previously published (CanmetMATERIALS, 2010; Shen, Gianetto, & Tyson, 2008), they will be included here since the comparison between the *J*-integrals is indispensable to this paper.

For the calculation of the *J*-integral from the CMOD, J_{CMOD}, the same formulation of ASTM E1820-11e2 (*J*-elastic + *J*-plastic) is used for SE(T) specimens; where $J_{el,i}$ is the elastic component of the *J*-integral and $J_{pl,i}$ is the plastic component, used in:

$$J_i = J_{el,i} + J_{pl,i} \,. \tag{1}$$

In Eq. (1), i is the index of the specific unload/reload cycle, and $J_{el,i}$ is given by:

$$J_{el,i} = \frac{K_i^2\left(1-\nu^2\right)}{E}, \tag{2}$$

with

$$K_i = \left(\frac{F_i\sqrt{\pi a_i}}{\sqrt{BB_N}W}\right)\times G\left(\frac{a_i}{W}\right), \tag{3}$$

E = Young's modulus, and ν = Poisson's ratio at the test temperature.

In Eq. (3), F_i is the force at the beginning of the unload/reload cycle, and

$$G\left(\frac{a_i}{W}\right) = \sum_{i=1}^{12} t_i\left(\frac{a}{W}\right)^{i-1} . \tag{4}$$

The coefficients of the polynomial regression (t_i) can be found in (Shen et al., 2008) .

$J_{pl,i}$ is expressed as:

$$J_{pl,i} = \left(J_{pl,i-1} + \frac{\eta_{CMOD,i-1}}{b_{i-1}}\times\frac{A_{pl,i}-A_{pl,i-1}}{B_N}\right) \times\left[1-\frac{\gamma_{LLD,i-1}\left(a_i-a_{i-1}\right)}{b_{i-1}}\right], \tag{5}$$

where b, the ligament size, is given by $(W - a)$, A_{pl} is the plastic area under the Force-CMOD curve, and the parameters η_{CMOD} and γ_{LLD} were obtained by FEA with the 2-D plane-strain assumption (Shen & Tyson, 2009). Both parameters are expressed as high-order polynomial functions of a/W.

The equation used for the determination of crack size based on CMOD elastic UC (C_i) measurements is

$$\frac{a_i}{W} = \sum_{i=0}^{8} r_i U_i \,, \tag{6}$$

where

$$U_i = \frac{1}{1+\sqrt{B_e C_i E}}, \tag{7}$$

$$B_e = B - \frac{\left(B-B_N\right)^2}{B}, \tag{8}$$

and r_i are the coefficients of a polynomial least-squares fitting function.

The incremental crack size (a_i) was calculated from the CMOD UC (ΔCMOD/ΔForce), with use of the central 80 % of the data to eliminate contribution from plastic deformation and machine or fixture effects on the data.

The value of the elastic UC (C_i) to be used in Eq. (7) must be corrected for specimen rotation as the center of the remaining ligament moves away from the load-line (Joyce & Link, 1995):

$$C_{c,i} = \frac{C_i}{F_{r,i}}, \tag{9}$$

where $C_{c,i}$ is the rotation-corrected compliance. The rotation correction factor[1], (F_r), has been established by 2-D plane-strain FEA, also evaluated with 3-D FEA, showing similar results (Shen & Tyson, 2009)

[1] F_r was inverted by typographical error in (Shen & Tyson, 2009).

for a clamped SE(T) specimen with H/W = 10 and a/W between 0.2 and 0.5, as

$$F_{r,i} = 1 - 0.165 \frac{a_0}{W} \left(\frac{F_i}{F_Y} \right). \quad \textbf{(10)}$$

All the tests performed were analyzed in accordance with the procedures for J-R curve testing prescribed by ASTM E1820, including the adjustment of the initial crack size by fitting all (J_i,a_i) pairs before maximum force with the following equation:

$$a = a_{0q} + \frac{J}{2\sigma_Y} + BJ^2 + CJ^3, \quad \textbf{(11)}$$

where a_{0q} is the adjusted initial crack size. The coefficients B and C are least-squares fitting constants. In cases of apparent negative crack growth, all data points preceding the minimum calculated crack size were excluded from the regression.

J-INTEGRAL FROM SURFACE STRAINS

Experimental techniques for measuring the J-integral by strain gages date back to the 1980's (Dodds & Read, 1985, 1990; D. Read, 1983; D. T. Read, 1988), representing experimental use of original theories developed by Rice (1968), thereby directly implementing the reported mathematical definition of J.

$$J = \oint_\Gamma W_\varepsilon dy - \vec{T} \cdot d\vec{v}/dx \, ds, \quad \textbf{(12)}$$

where, x and y are position coordinates. W_ε is the strain energy density function, $\vec{T}$ is the traction vector, (force vector per unit area), $\vec{v}$ is the displacement vector and ds is an element of arc length along the contour (Γ).

The relationship between the physical specimen, exaggerated deformation, coordinates and measurement scheme are illustrated in Figure 8. The contour used for the present experimental evaluation of J was a far-field contour. It followed the specimen surfaces along the axial center-line beginning and ending at opposing edges of the original notch. The Contour encompassed the front-face surface, through thickness and back-face surface of the specimen symmetric about the notch plane spaced at 70 mm (4W).

J-integral values were calculated per Eq. 12 for each row in the digital data record containing, load, strain and displacement values. First, a reference function giving the strain energy density as a function of axial true strain was determined from the uniaxial stress strain data. This is possible because the strain gages are surface mounted far from the crack tip, and it is assumed that there are no transverse-direction stresses at the strain gage locations.

The uniaxial stress-strain curve is then used to evaluate reference values of W_ε as a function of applied strain, ε_y from

$$W(\varepsilon) = \int_0^\varepsilon \sigma_{uss} d\varepsilon_{uss}, \quad \textbf{(13)}$$

where, σ_{uss} and ε_{uss} are the true stress and true strain values from the uniaxial stress-strain curve for this material.

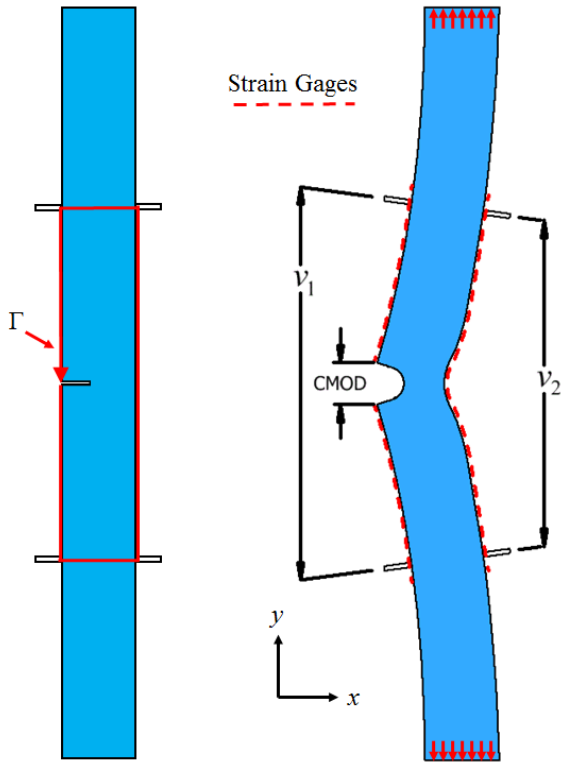

Figure 8. Schematic depiction of an undeformed SE(T) specimen and exaggerated deformation in the fully plastic regime. Shown are the contour (Γ) and the locations of the strain and displacement instrumentation.

Strain values as measured along the front- and back-faces of the specimen were fitted to cubic splines as a function of gage position (y-direction). The spline coefficients were then used to calculate strain values (ε_y) for each y-direction contour segment as a function of y with 0.5 mm increments. At each of these y values a strain energy density W_ε was obtained by entering the strain (ε_y) into the reference strain energy density function, Eq. 13. The y-direction integrations of the W_ε values were carried out by use of the trapezoidal rule.

The second term of the J definition (Eq. 12), applicable to the horizontal segments of the contour, was approximated by the product of the average tensile stress and the difference in axial displacement from the front-face to the back-face; this relationship is shown in Eq. 14,

$$-\int_\Gamma \vec{T} \cdot d\vec{v}/dx \, ds = \frac{P}{A}(v_1^s - v_2^s). \quad \textbf{(14)}$$

The values v_1^s and v_2^s represent the values of the front- and back-face extensions as measured on the surface of the specimen obtained by linear interpolation between v_1 and v_2, see Figure 8. This scheme utilizes the cancellation of dx and ds in Eq. 12 (with the signs accounted for) along the horizontal contour segments. It also accounts for the sign differences of the traction-bending term and the increment of v between the lower

and upper segments of the contour. Note that if $d\vec{v}/dx$ is constant through the specimen from the front-face to the back-face, no error is encountered in this approximation of $\vec{T}$ as the magnitude of the average tensile stress.

To illustrate this physically, Figure 9 shows the FEA output at 1.05 mm CMOD indicating where the highest stress values occur. The upper and lower boundaries of the contour with respect to the *y*-direction coincide with the location of the surface displacement measurements (v_1^s and v_2^s). This FEA simulation was also used to check the assumption that $d\vec{v}/dx$ was constant through the thickness of the specimen. Evaluating the FEA model output at these locations shows a nearly constant value for $d\vec{v}/dx$ as shown in Figure 10 for a CMOD of 1.05 mm.

By use of traction and $d\vec{v}/dx$ values from the FEA the traction-bending term was evaluated with and without the assumption of constant $d\vec{v}/dx$. The difference was less than 1 % which allows an estimation of less than 0.3 % error propagated to the J_{SG} calculation.

In these specimens, the contributions of the two terms to the *J*-integral were within a factor of two (2) of each other over essentially the full range of the reported *J*-integral data.

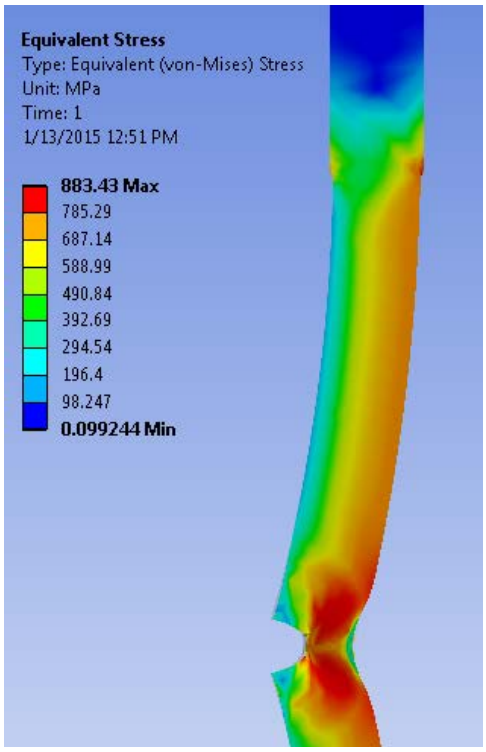

Figure 9. FEA output indicating the equivalent stress along the specimen at a CMOD opening of 1.05 mm. For viewing clarity, displacements are shown exaggerated by a factor of 10 (relative to the actual displacements).

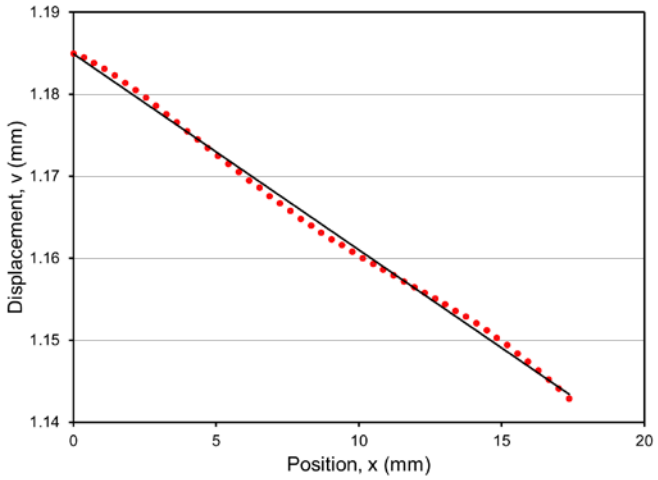

Figure 10. Plot of displacement vs. position (through width), derived from the front- and back-face extensometers. A straight line indicates a constant $d\vec{v}/dx$, allowing for the average stress in the remaining ligament to be used as the traction-bending term for the *J*-integral.

To be clear, the presence of side grooves was ignored in the computation of the *J*-integral since measurements were only taken along the axial centerline. Furthermore, the definition of the *J*-integral and the proof of path-independence (Rice, 1968) is for two-dimensional deformation and the presence of the side grooves makes the actual test a more complex three-dimensional condition. It is recognized that this will account as one contribution to the differences between J_{CMOD} and those presented here.

Since a *J*-integral value is available at each increment of crack growth, the same CMOD UC method was conveniently superimposed on the strain data for evaluation and comparison. The procedure as described so far allowed J_{SG} values to be obtained until the peak strain reached approximately 0.025 mm/mm, where many strain gages began to fail due to the limitations of surface mounted strain gages. This procedure resulted in *J*-integral values available for correlation to CMOD and crack extension.

RESULTS

The first validity check for this method required an examination of the strain data over the course of the test. Since the back-face strains were expected to, and did, have the largest indicated strain values, they are presented here exclusively. A plot of the strains along the back-face of a specimen is shown in Figure 11; the position references the notch-plane. It is notable that the peak strains are not symmetric about the notch-plane. This is a measured effect that FEA would not have simulated for a homogenous material, with an ideal geometry. Incipient necking and non-uniform plasticity is the most likely source for this measured effect.

The J_{SG} values up to the first strain gage failure are compared to J_{CMOD} values in Figure 12. The J_{SG} values match the J_{CMOD} values very well initially and begin to diverge to approximately 85 % of the J_{CMOD} values with increasing CMOD.

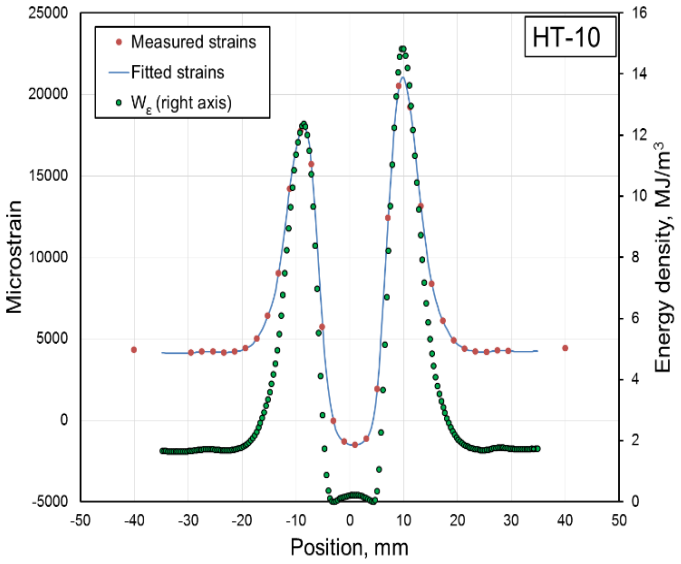

Figure 11. Measured strain values along the back face in specimen HT-10 at a CMOD of 0.80 mm. Also shown are the local energy density values deduced from the fitted strains, which were used in the *J*-integral calculation.

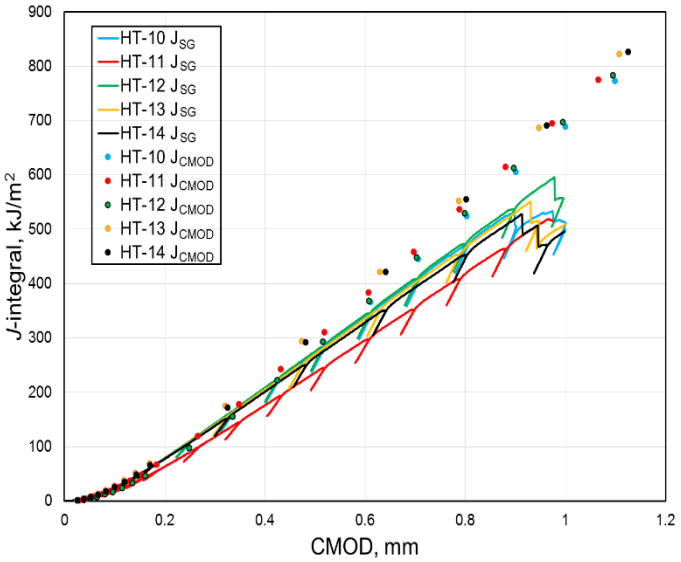

Figure 12. Plot comparing J_{SG} and J_{CMOD} up to the first strain gage failures in each test.

An attempt was made to roughly estimate the J_{SG} values past the point of strain gage failure by extrapolating the strain gage results. This procedure must be considered with caution, because the gages that numerically contribute the most to the *J*-integral are the ones that fail first. Simple linear extrapolation was used in place of data lost from failed gages. The extrapolation considers only the strains above the plastic limit of about 0.005 mm/mm to avoid complications from the elastic-plastic transition. A sample set of extrapolated strain data is shown in Figure 13.

As a check on this extrapolation scheme, the same extrapolated strain values were used to calculate the total tensile displacement along the specimen at each data point. The results based on the back-face extensometer measurements are shown in Figure 14.

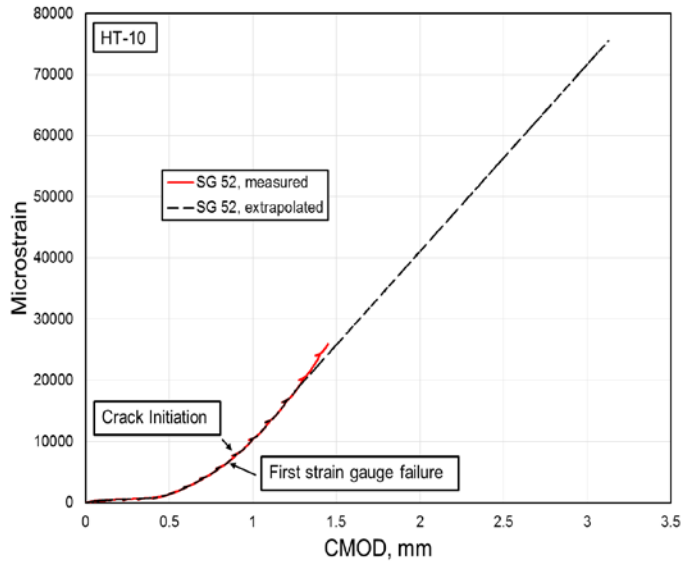

Figure 13. Plot of strain vs. CMOD for one remote strain gage on a specimen underpinning the need for high-strain measurement capability. The strain gages located in the region of highest strain failed very close to the point of crack initiation.

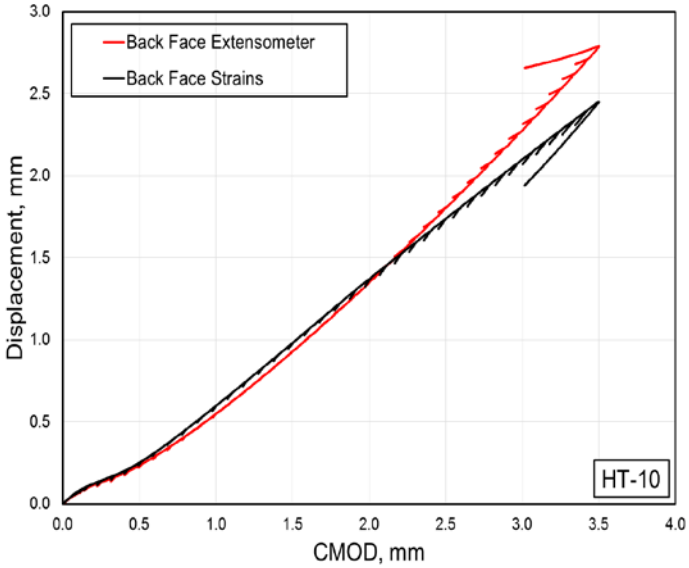

Figure 14. Plot of displacement vs. CMOD comparing extension calculated from extrapolated strain gage data and directly measured CMOD. Perfect extrapolation would result in a perfect match.

The generally close agreement shown in this figure between the displacements from the extrapolated strains and the displacements from the extensometers allows optimism that the J_{SG} values from extrapolated strains are reasonable.

The *J*-R curves calculated for the five SE(T) specimens based on J_{CMOD} data, and based on the J_{SG} method (with actual and extrapolated strains), are compared in Figure 15. Again, the J_{SG} values diverge to 15 % - 20% below the J_{CMOD} values.

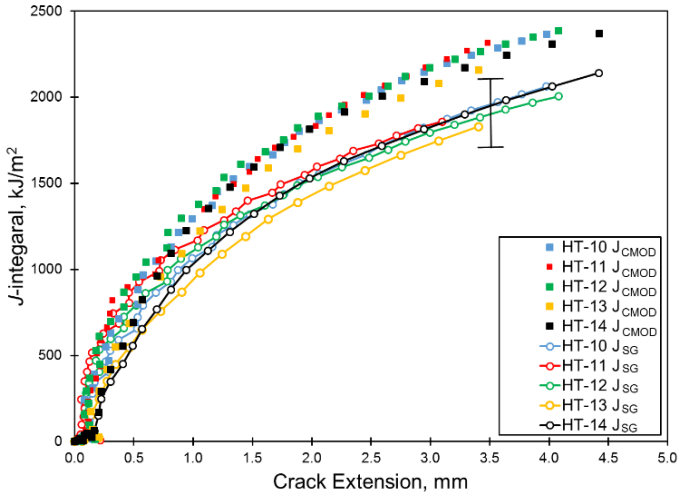

Figure 15. *J*-R curves generated from both methods of evaluating *J*-integral for each specimen tested. The error bar represents the estimated uncertainty in the J_{SG} values propagated from the uncertainties in the extrapolated strains.

DISCUSSION

Experimental Considerations

The technique presented here measured the actual strains that contribute to the evaluation of a contour *J*-integral. Evaluation of the *J*-integral by way of surface strains was shown here to be highly dependent on the survival of the strain gages throughout the test. An extrapolation scheme can be used and provides data that falls well within the 20 % standard deviation reported by Tyson and Gianetto (2013). Ultimately however, the method can and should use strain data obtained from a method that collects valid strains far past the plasticity limits of the material (*e.g.*, Digital Image Correlation).

It is acknowledged and readers are cautioned that determining J_{SG} is not a surrogate for determining J_{CMOD}.

Theoretical Considerations

An ideal case for experimental and numerical analysis would be exact path independence. An important condition of path-independence is that of linear or non-linear elasticity, interpreted as reversibility of the stress-strain curve. In the case of an actual test, cyclic loading and more importantly the plasticity in the region of a growing crack diminishes the mathematical path-independence of the *J*-integral. Furthermore, the 3D nature of the strain field also invalidates the path independence mathematically proven in 2D plain strain or plane stress conditions (Rice, 1968). Regardless of true path independence, the *J*-integral remains a valuable measure of fracture toughness applied to structural assessment.

FEA was performed on straight sided specimen models (no side-grooves) to visualize the plasticity occurring at the crack tip. The static-structural FEA again used a bilinear isotropic material, with small strains, allowing non-linear effects and without special crack tip treatments. For the purposes of this study, FEA was used to visualize effects and relate measured data to physical responses in the specimen. The FEA results presented here do not represent a comprehensive parametric study. Figure 16 shows the equivalent plastic strain for said specimen at a CMOD opening of 1.05 mm. Note the stark difference in strains at the crack tip from the relatively low strains at the surface. Therefore, comparisons between the J_{SG} and J_{CMOD} depend on the details of the evaluation of *J* in both cases, specifically related to plasticity.

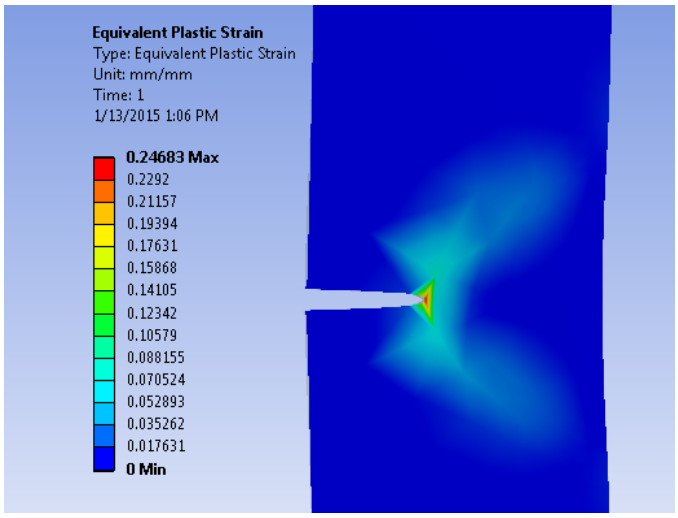

Figure 16. FEA output indicating the equivalent plastic strain at the crack tip at a CMOD opening of 1.05 mm.

Another issue of particular interest is the effect of the side grooves where remaining material may add constraint to the advancing crack. It is well established that the plane strain approximation at the crack tip is valid for small crack extensions. Caution is warranted and assumptions must be further validated for large crack extensions especially with high strain hardening materials and large scale plasticity.

In order to relate the J_{SG} results to the J_{CMOD} results, the condition of plane strain or plane stress and plasticity must be addressed. In the case of evaluating *J*-integral from directly measured surface strain gradients it is impossible to determine if plane strain or plane stress conditions are present at different locations in the specimen. To calculate *J* from strain gradients that would be comparable to *J* from CMOD at a common load, the multitude of assumptions that allow for the calculation of each require further examination. Additional modelling and analysis of this mixed structural condition is the subject of on-going investigations. The goal is to determine the crack tip strain energy (average *J* across the 3D crack front) without the ability to directly measure the full thickness stress and strain distribution.

CONCLUSIONS

A direct measurement of the *J*-integral is presented in this paper for comparison to an analytically derived *J*-integral. The direct measurement method uses surface mounted strain gages and extensometers for validation. The analytical derivation of the *J*-integral uses the CMOD and is from the published work of Shen et al. (2008). Both methods were successfully applied to the same specimens assuring a direct comparison with the same geometries and test conditions.

Experimental measurement limitations of strain by use of surface mounted strain gages presented some difficulty in the analysis which was overcome by linearly extrapolated strains with acceptable results.

Continued work based on this method is being undertaken with digital

image correlation (DIC). A significant advantage of DIC is that multiple contours can be evaluated and compared. Furthermore, DIC also provides plastic strain measurements far beyond the limits of surface mounted strain gages.

Differences between the directly measured *J*-integral and the analytically derived *J*-integral arise due to the fact that the two methods evaluate two different quantities. Specifically the J_{CMOD} is a measure of the plane strain conditions closely approximated at the crack tip in contrast to the J_{SG} value interrogating far-field response to loading. For limited plasticity and crack extension the *J*-integral calculated from surface strain gradients is comparable to the *J*-integral calculated from CMOD measurements with results diverging as both plasticity and crack extension increase. The present results quantify this divergence for an important specimen geometry and relevant material to the pipeline industry. The errors associated with the direct measurement method do not significantly contribute to the differences presented.

The direct measurement approach presented here may prove to be a useful tool to evaluate complex geometries and crack paths such as those encountered when testing welds. This approach may also be useful to investigate transferability between standardized small-scale test geometries and full scale conditions

ACKNOWLEDGEMENTS

Funding for this research was provided by the U.S. Department of Commerce, National Institute of Standards and Technology's Pipeline Safety Project. The authors are grateful to J.A. Gianetto and to W.R. Tyson of CanmetMATERIALS for providing test specimen blanks, and their keen interest and correspondence related to this work. Finally, the authors are indebted to engineering technicians Ken Talley and Ross Rentz for their expert support in these experiments.

REFERENCES

ASTM. (2013). E1820-13 Standard Test Method for Measurment of Fracture Toughness. West Conshohocken, PA, USA: ASTM International.

BSI. (1991). BS7448-1 Fracture Mechanics Toughness Tests - Part 1: Method for determination of KIc, Critical CTOD and Critical J Values of Metallic Materials: BSI.

CanmetMATERIALS. (2010). Recommended Practice: Fracture Toughness Testing Using SE(T) Samples With Fixed-Grip Loading.

Chao, Y. J., Yang, S., & Sutton, M. A. (1994). On the fracture of solids characterized by one or two parameters: theory and practice. *Journal of the Mechanics and Physics of Solids*, 42(4), 629-647.

Chao, Y. J., & Zhu, X.-K. (2000). Constraint-modified J− R curves and its application to ductile crack growth. *International Journal of Fracture*, 106(2), 135-160.

Cravero, S., & Ruggieri, C. (2007). Estimation Procedure of J-Resistance Curves for SE(T) Fracture Specimens Using Unloading Compliance. *Engineering Fracture Mechanics*, 74(17), 2735-2757.

DNV-RP-F108. (2006). Recommended Practice: Fracture Control for Pipeline Installation Methods Introducing Cyclic Plastic Strain: Det Norske Veritas.

Dodds, R. H., & Read, D. T. (1985). Experimental and Analytical Estimates of the J-integral for Tensile Panels Containing Short Center Cracks. *International Journal of Fracture*, 28(2), 39-54.

Dodds, R. H., & Read, D. T. (1990). Experimental and Numerical Studies of the J-integral for a Suface Flaw. *International Journal of Fracture*, 43(1), 47-67.

ExxonMobil. (2010). Measurement of Crack Tip Opening Displacement (CTOD) - Fracture Resistance Curves Using Single-Edge Notched Tension (SENT) Specimens.

Hertelé, S., Verstraete, M., Denys, R., & O'Dowd, N. (2014). J-integral analysis of heterogeneous mismatched girth welds in clamped single-edge notched tension specimens. *International Journal of Pressure Vessels and Piping*, 119, 95-107.

ISO. (2007). 12135 Metallic materials–Unified method of test for the determination of quasistatic fracture toughness. International Organization for Standardization.

Joyce, J. A., & Link, R. E. (1995). Effect of Constraint on Upper Shelf Fracture Toughness. *ASTM Special Technical Publication 1256*.

Joyce, J. A., & Link, R. E. (1997). Application of two parameter elastic-plastic fracture mechanics to analysis of structures. *Engineering Fracture Mechanics*, 57(4), 431-446.

Kalyanam, S., Wilkowski, G. M., Shim, D.-J., Brust, F. W., Hioe, Y., Wall, G., & Mincer, P. (2010). *Why Conduct SEN (T) Tests and Considerations in Conducting/Analyzing SEN (T) Testing.* Paper presented at the *International Pipeline Conference*, Calgary, Alberta, Canada.

Kim, Y., Zhu, XK, Chao, YJ. (2001). Quantification of constraint on elastic–plastic 3D crack front by the J– A2 three-term solution. *Engineering Fracture Mechanics*, 68(7), 895-914.

Liu, S., & Chao, Y. (2003). Variation of fracture toughness with constraint. *International Journal of Fracture*, 124(3-4), 113-117.

Mathias, L., Sarzosa, D., & Ruggieri, C. (2013a). Effects of specimen geometry and loading mode on crack growth resistance curves of a high-strength pipeline girth weld. *International Journal of Pressure Vessels and Piping*, 111, 106-119.

Mathias, L., Sarzosa, D., & Ruggieri, C. (2013b). *Evaluation of Ductile Tearing of X-80 Pipeline Girth Welds Using SE (T), SE (B) and C (T) Fracture Specimens.* Paper presented at the *Pressure Vessels and Piping Conference*, Paris, France.

Paredes, M., & Ruggieri, C. (2011). *Effects of Weld Strength Mismatch on J and CTOD Estimation Procedures for SENT Fracture Specimens Based on Plastic Eta-Factors.* Paper presented at the *International Conference on Ocean, Offshore and Arctic Engineering*, Rotterdam, The Netherlands.

Park, D.-Y., Tyson, W. R., Gianetto, J. A., Shen, G., & Eagleson, R. S. (2010). *Evaluation of Fracture Toughness of X100 Pipe Steel Using SE(B) and Clamped SE(T) Single Specimens.* Paper presented at the *International Pipeline Conference*, Calgary, Alberta, Canada.

Park, D.-Y., Tyson, W. R., Gianetto, J. A., Shen, G., Eagleson, R. S., Lucon, E., & Weeks, T. S. (2011a). Small-Scale Low-Constraint Fracture Toughness Test Results *Final Report 277-T-06 to DOT/PHMSA*, *http://primis.phmsa.dot.gov/matrix/FilGet.rdm?fil=7330*.

Park, D.-Y., Tyson, W. R., Gianetto, J. A., Shen, G., Eagleson, R. S., Lucon, E., & Weeks, T. S. (2011b). Small Scale Low Constraint Fracture Toughness Test Discussion and Analysis *Final Report 277-T-07 to DOT/PHMSA*, *http://primis.phmsa.dot.gov/matrix/FilGet.rdm?fil=7331*.

Pisarski, H. G. (2010). *Determination of pipe girth weld fracture toughness using SENT specimens.* Paper presented at the *International Pipeline Conference*, Calgary, Alberta, Canada.

Pisarski, H. G., & Wignal, C. M. (2002). *Fracture Toughness Estimation for Pipeline Girth Welds.* Paper presented at the *International Pipeline Conferenc*e, Calgary, Alberta, Canada.

Pussegoda, L. N., Tiku, S., Tyson, W. R., Park, D.-Y., Gianetto, J. A., Shen, G., & Pisarski, H. G. (2013). *Comparison of Resistance Curves from Multi-Specimen and Single Specimen SEN(T) Tests.* Paper presented at the *International Offshore and Polar Engineering Conference*, Anchorage, AK, USA.

Read, D. (1983). Experimental method for direct evaluation of the J-contour integral. *ASTM Special Technical Publication 791*, 199-213.

Read, D. T. (1988). J-integral values for Small Cracks in Steel Panels. *ASTM Special Technical Publication 945*.

Rice, J. R. (1968). A path independent integral and the approximate analysis of strain concentration by notches and cracks. *Journal of applied mechanics*, 35(2), 379-386.

Ruggieri, C. (2012a). *Constraint effects on ductile crack growth in SE (T) and SE (B) specimens with implications for assessments of tearing resistance.* Paper presented at the *International Pipeline Conference*, Calgary, Alberta Canada.

Ruggieri, C. (2012b). Further results in J and CTOD estimation procedures for SE (T) fracture specimens–Part I: Homogeneous materials. *Engineering Fracture Mechanics*, 79, 245-265.

Sarzosa, D. B., & Ruggieri, C. (2013). *Further Insights on J-R Curve Behavior in Pipeline Steels Using Low Constraint Fracture Specimens.* Paper presented at the *Pressure Vessels and Piping Conference*, Paris, France.

Shen, G., Gianetto, J. A., & Tyson, W. R. (2008). Development of Procedure for Low-Constraint Toughness Testing Using a Single-Specimen Technique *MTL Report No. 2008-18 (TR)*: CanmetMATERIALS.

Shen, G., & Tyson, W. R. (2009). Crack Size Evaluation Using Unloading Compliance in Single-Specimen Single-Edge Notched Tension Fracture Toughness Testing. *Journal of Testing and Evaluation*, 37(4).

Silva, L. A. L., Cravero, S., & Ruggieri, C. (2006). Correlation of fracture behavior in high pressure pipelines with axial flaws using constraint designed test specimens. Part II: 3-D effects on constraint. *Engineering Fracture Mechanics*, 73(15), 2123-2138.

Tang, H., Macia, M., Minnaar, K., Gioielli, P., Kibey, S., & Fairchild, D. (2010). *Developement of the SENT Test for Strain-Based Design of Welded Pipelines.* Paper presented at the *International Pipeline Conference*, Calgary, Alberta, Canada.

Tyson, W. R., & Gianetto, J. A. (2013). *Low-Constraint Toughness Testing: Results of a Round-robin on a Draft SE(T) Test Procedure.* Paper presented at the *Pressure Vessels and Piping Conference*, Paris, France.

Verstraete, M., Hertelé, S., Denys, R., Van Minnebruggen, K., & De Waele, W. (2014). Evaluation and interpretation of ductile crack extension in SENT specimens using unloading compliance technique. *Engineering Fracture Mechanics*, 115, 190-203.

Wang, E., Zhou, W., Shen, G., & Duan, D. (2012). *An Experimental Study on J (CTOD)-R Curves of Single Edge Tension Specimens for X80 Steel.* Paper presented at the *International Pipeline Conference*, Calgary, Alberta, Canada.

Weeks, T. S., & Lucon, E. (2014). *Direct Comparison of Single-Specimen Clamped SE(T) Test Methods on X100 Line Pipe Steel.* Paper presented at the *International Pipeline Conference*, Calgary, Alberta, Canada.

Weeks, T. S., McColskey, J. D., Read, D. T., & Richards, M. D. (2013). *Fracture toughness instrumentation techniques for single-specimen clamped SE(T) tests on X100 line pipe steel: Experimental Setup.* Paper published at the *Pipeline Technology Conference*, Ostend, Belgium.

Zhu, X.-K., & Joyce, J. A. (2012). Review of fracture toughness (G, K, J, CTOD, CTOA) testing and standardization. *Engineering Fracture Mechanics*, 85, 1-46.

Zhu, X.-K., & McGaughy, T. (2014). *A Review of Fracture Toughness Testing and Evaluation Using SENT Specimens.* Paper presented at the *International Pipeline Conference*, Calgary, Aberta Canada.